HMG Advance Access published November 7, 2008



# The *Drosophila* homologue of the Angelman syndrome ubiquitin ligase regulates the formation of terminal dendritic branches

Yubing Lu[1,†], Fay Wang[1,2,†], Yan Li[1,3,†], Jacob Ferris[1], Jin-A Lee[1], Fen-Biao Gao[1,*]

[1]Gladstone Institute of Neurological Disease and Department of Neurology, University of California, San Francisco, CA 94158 USA.

[2]Current address: Advanced Cell Diagnostics, Fremont, CA 94555 USA.

[3]Current address: Department of Neurology, Northwestern University, Chicago, IL 60611 USA.

[†] These authors contributed equally to this work.

*To whom correspondence should be addressed at: Gladstone Institute of Neurological Disease, 1650 Owens Street, San Francisco, CA 94158. Tel: (415) 734-2514; Fax (415) 355-0824; Email: fgao@gladstone.ucsf.edu

© The Author 2008. Published by Oxford University Press. All rights reserved.
For permissions, please e-mail: journals.permissions@oxfordjournals.org

**ABSTRACT**

Angelman syndrome is a severe neurodevelopmental disorder mostly caused by loss-of-function mutations in the maternal allele of *UBE3A*, a gene that encodes an E3 ubiquitin ligase. *Drosophila* UBE3A (dUBE3A) is highly homologous to human UBE3A at the amino acid sequence level, suggesting functional conservation. We generated *dUBE3A*-null mutant fly lines and found that dUBE3A is not essential for viability. However, loss of dUBE3A activity reduced dendritic branching of sensory neurons in the peripheral nervous system and slowed the growth of terminal dendritic fine processes. Several lines of evidence indicated that dUBE3A regulates dendritic morphogenesis in a cell-autonomous manner. Moreover, overexpression of dUBE3A also decreased dendritic branching, suggesting that the proper level of dUBE3A is critically important for the normal dendritic patterning. These findings suggest that dendritic pathology contributes to neurological deficits in patients with Angelman syndrome.

## INTRODUCTION

In many neurons, dendritic branches account for more than 90% of the neuronal surface that receives synaptic input from other neurons. Therefore, the proper formation of dendritic branching patterns is critically important for neuronal function and connectivity. Despite considerable progress in understanding the molecular and genetic pathways that control different aspects of dendritic morphogenesis (1–4), little is known about how abnormalities in dendritic formation contribute to neurodevelopmental disorders.

Angelman syndrome (AS) is a severe developmental brain disorder characterized by mental retardation, seizures, abnormal gait, frequent laughter, and other abnormalities (5). At least four genomic abnormalities cause AS (6, 7). Most patients have de novo deletions of about 4 Mb on maternal chromosome 15q11-q13. Another genomic abnormality, paternal uniparental disomy (UPD) on chromosome 15, results in two copies of paternal chromosomes but no maternal copy. A third abnormality, found in a small group of patients, is caused by paternal methylation of both paternal and maternal copies of chromosome 15q11-q13, resulting in loss of expression of the maternal copy. The fourth abnormality is loss-of-function point mutations in *UBE3A*, which has been found in some AS patients with classical symptoms. These genetic evidence indicate that *UBE3A* is primarily responsible for many if not all cases of AS (8, 9).

*UBE3A* encodes E6-AP ubiquitin ligase, a binding partner of the E6 protein of human papilloma virus that promotes the degradation of the p53 oncoprotein (10, 11). *UBE3A* is imprinted in the brain, especially in the hippocampus and cerebellum (12–14). Homozygous *UBE3A* knockout mice are growth-retarded and have reduced survival on different genetic backgrounds (15). Mice with maternal deficiency of *UBE3A* and a normal copy of the paternal gene have defects in context-dependent learning and long-term potentiation (15). Interestingly, the molecular and cellular deficits of an AS mouse model can be rescued by reducing inhibitory

phosphorylation of αCAMKII (16). Loss of maternal *UBE3A* appears to reduce spine density and length on hippocampal neurons (17). However, it is unclear whether the formation of terminal fine dendritic branches is affected.

*Drosophila* has been used successfully over the years as an excellent model system to understand the genes and molecular pathways that are misregulated in human disease conditions (18, 19). In the *Drosophila* genome, one gene, *CG6190*, encodes a protein highly homologous to human UBE3A (hUBE3A). *Drosophila UBE3A* (*dUBE3A*) contains eight exons that encode a protein with 973 amino acids. The C-terminal 350–amino acid HECT domains of dUBE3A and hUBE3A share 62% identity, suggesting functional conservation (20). In this study, we generated mutant flies lacking *dUBE3A* and investigated its in vivo function in dendritic morphogenesis, especially the formation of terminal fine dendritic branches.

## RESULTS

### Generation of *dUBE3A* mutant flies

To examine the phenotypes of *dUBE3A* loss-of-function mutant alleles, we generated fly lines in which dUBE3A was not expressed. *dUBE3A* is located on chromosome 3L and flanked by two previously uncharacterized genes, *CG6199*, which encodes a protein homologous to procollagen-lysine 2-oxoglutarate 5-dioxygenase, and *CG7600*, which encodes a conserved protein of unknown function (Fig. 1A). From the Bloomington Stock Center, we obtained a fly line (*EP3214*) containing an EP element in the first exon of *dUBE3A*, 293 nt upstream of the ATG start codon (Fig. 1B). This P-element insertion did not significantly reduce *dUBE3A* expression (data not shown).

Our phenotypic analysis relies heavily on the UAS-Gal4 system (21), and the presence of Gal4 drivers will likely lead to overexpression of *dUBE3A* through the UAS elements in the EP sequence (Fig. 1B). Therefore, the EP line itself is not suitable for our genetic analysis. To generate loss of function mutant alleles, we used a P-element local hop-out mutagenesis approach. First, the *EP3214* line was outcrossed with $w^{1118}$ flies for several generations to eliminate the background lethal mutation(s) on chromosome 3. Isogenic adult flies homozygous for *EP3214* were viable and fertile and were mated with flies expressing transposase. In most cases, *EP3214* was excised without any damage to the genomic region (e.g., line Δ*3-9*) (Fig. 1B). In a few instances, genomic deletions occurred near the insertion site of the EP element, generating potential *dUBE3A*-null alleles (Fig. 1B). PCR analysis confirmed genomic deletions in the first or second exon of *dUBE3A* and the first exon of *CG7600* in some mutant lines (e.g., line Δ*3-8*). Fortuitously, in line Δ*15-8*, a 1.1-kb DNA fragment from the EP element was left behind in the genome after the hop-out (Fig. 1B), creating a new insertional mutant allele (see below).

Adult flies that were homozygous for all the deletion mutations or the 0.8-kb insertion were viable. To confirm the presence of *dUBE3A*-null alleles, we performed two experiments. First, we analyzed total RNA from homozygous mutant flies by quantitative PCR. As expected, the level of *dUBE3A* mRNA was normal in line Δ*3-9*, dramatically reduced in line Δ*15-8*, and absent in line Δ*3-8* (Fig. 2A). Earlier PCR analysis on the genomic DNA indicated that all the deletion mutants also affected *CG7600* (Fig. 1B). Indeed, *CG7600* mRNA was undetectable in line Δ*3-8* (Fig. 2A). However, the 0.8-kb insertion in the first exon of *dUBE3A* specifically reduced the expression of *dUBE3A* mRNA without affecting the expression of *CG7600* mRNA (Fig. 2A), providing a useful strong *dUBE3A* loss of function allele for further phenotypic analysis. Second, we generated rabbit polyclonal antibodies against the first 300 amino acids of dUBE3A and

confirmed, by western blot analysis, the absence of the dUBE3A protein in several mutants, including Δ*3-8* and Δ*15-8* (Fig. 2B).

**Reduced dendritic growth and branching in *dUBE3A* mutant larvae**

To examine the role of dUBE3A in dendritic morphogenesis, we used dendritic arborization (DA) neurons in the *Drosophila* peripheral nervous system as an in vivo assay system. *Drosophila* sensory neurons have been widely used to dissect the genetic pathways that control dendritic morphogenesis (4). Among these neurons, ddaC in the dorsal cluster and similar neurons in other clusters in the same segment of *Drosophila* third instar larvae elaborate extensive dendritic arbors that cover the whole body wall. We used $Gal4^{477}$ to label ddaC neurons with GFP in control and *dUBE3A* mutant larvae and quantified the number of terminal branches as described (22). For control larvae, we used either $w^{1118}$ or precise hop out lines (such as Δ*3-9*) that did not show a difference in dendritic branching of ddaC neurons. In contrast, in $dUBE3A^{\Delta 15\text{-}8}$ homozygous mutant third instar larvae, the number of terminal branches was significantly reduced (309.9 ± 17.8, n = 13 vs. 533.0 ± 22.6, n = 11, $p < 0.001$) (Fig. 3B, D), although the overall branching patterns of ddaC neurons in the A3 segment, especially the primary and secondary branches, remained the same as in wildtype larvae (Fig. 3A, B).

To further confirm this phenotype, we examined *dUBE3A* mutant larvae transheterozygous with Δ*3-8* and Δ*15*-8 alleles revealed a similar dendritic phenotype (Fig. 3C, D). Moreover, in wildtype larvae, the terminal dendritic branches of ddaC neurons extended to target the body wall receptive field more or less evenly (Fig. 3A). However, these branches were much shorter in homozygous $dUBE3A^{\Delta 15\text{-}8}$ mutants and transheterozygous $dUBE3A^{\Delta 15\text{-}8}/dUBE3A^{\Delta 3\text{-}8}$, and patches of the target field were devoid of dendrites. Thus, dUBE3A is required for the proper growth and branching of terminal dendrites of ddaC neurons.

**dUBE3A regulates dendritic morphogenesis in a cell-autonomous manner**

To determine if the dendritic phenotype in *dUBE3A* mutant larvae arose through effects of dUBE3A in neurons or through a non-cell-autonomous mechanism, we used RNAi to knock down *dUBE3A* expression only in ddaC neurons. First, we tested the effectiveness of different UAS-*dUBE3A* RNAi lines generated in our lab or obtained from the Vienna *Drosophila* RNAi Center (VDRC). The RNAi constructs were expressed in all cell types under the control of *tubulin*-Gal4, and proteins from adult fly heads were analyzed by western blot. UAS-*dUBE3A* RNAi (VDRC45875) and UAS-*dUBE3A* RNAi (VDRC45876) downregulated dUBE3A expression more effectively than several UAS-*dUBE3A* RNAi lines we generated (Fig. 4A). Polyclonal antibody against recombinant dUBE3A recognized two bands on western blot, both of which were absent in homozygous $dUBE3A^{\Delta 15\text{-}8}$ mutants and dramatically downregulated in flies expressing UAS-*dUBE3A* RNAi (VDRC45876), raising the possibility that the top band may be a result of post-translational modification. The biological significance of this modification remains to be determined.

To examine the developmental consequence of loss of dUBE3A activity, we targeted the expression of UAS-*dUBE3A* RNAi (VDRC45875) and UAS-*dUBE3A* RNAi (VDRC45876) to ddaC neurons using $Gal4^{477}$. To enhance the effects of RNAi, the RNAi constructs were expressed in the $dUBE3A^{\Delta 15\text{-}8}$/+ background. The resulting dendritic growth and branching phenotype was highly similar to that in *dUBE3A* mutant larvae. For instance, there were fewer terminal dendritic branches (VDRC45875, 362.1 ± 23.3, n = 9 vs. control 524.3 ± 22.6, n = 11, $p < 0.001$; VDRC45876, 383.7 ± 18.4, n = 10 vs. control 524.3 ± 22.6, n = 11, $p < 0.001$) (Fig. 4B–E).

To further test the cell-autonomous function of *dUBE3A*, we performed mosaic analysis with a repressible cell marker (MARCM) (23). This technique allows GFP labeling of single ddaC

neurons with defined genetic mutations in an otherwise wildtype larva. *dUBE3A* mutant ddaC neurons labeled by MARCM also exhibited a dendritic phenotype similar to that in mutant larva and in ddaC neurons expressing RNAi constructs (Fig. 5), further demonstrating that dUBE3A functions in a cell-autonomous manner to control dendritic growth and branching. When GFP-tagged dUBE3Awas expressed in ddaC neurons, the GFP signal was present throughout the dendritic trees (data not shown). This finding raises the possibility that dUBE3A regulates the abundance of its substrates locally to control the formation of terminal dendritic branches.

**dUBE3A is required for the proper dendritic formation of other neurons**

To extend our phenotypic analysis to other neurons in *Drosophila* larvae, we examined ddaE and ddaF neurons in the dorsal cluster. These sensory neurons extend smooth dendritic branches over a much smaller dendritic field than ddaC neurons (24, 25). MARCM analysis revealed that *dUBE3A* is also required cell-autonomously for proper branching of ddaE and ddaF neurons: the number of dendritic branches was decreased in ddaE neurons that were homozygous for the $dUBE3A^{\Delta 3\text{-}8}$ (27.1 ± 1.5, n = 7, vs. 31.8 ± 2.1, n = 13, $p < 0.05$) (Fig. 6B, D) or $dUBE3A^{\Delta 15\text{-}8}$ allele (22.0 ± 1.7, n = 8, vs. 31.8 ± 2.1, n = 13, $p < 0.01$) (Fig. 6C, D). MARCM-labeled ddaF neurons exhibited a similar phenotype (Fig. 6D). Expression of UAS-*dUBE3A* RNAi driven by $Gal4^{221}$ decreased the number of dendritic branches in both ddaE neurons (VDRC45876, 27.8 ± 1.2, n = 20 vs. control, 32.0 ± 1.0, n = 10, $p < 0.05$; VDRC45875, 29.2 ± 0.9, n = 9 vs. control 32.0 ± 1.0, n = 10, $p < 0.05$) (Fig. 6E–H). In ddaF neurons, a similar phenotype was observed (VDRC45876, 18.6 ± 1.0, n = 20 vs. control, 25.8 ± 1.3, n = 20, $p < 0.01$; VDRC45875, 19.9 ± 0.5, n = 9 vs. control 25.8 ± 1.3, n = 20, $p < 0.001$) (Fig. 6E–H). These results indicate that dUBE3A is required cell-autonomously for the proper branching of different neurons in the *Drosophila* PNS.

**Genetic interaction between *dUBE3A* and *eff* that encodes an E2 ligase**

ddaC neurons in *dUBE3A* mutants fail to completely prune their dendrites during early metamorphosis (Y. Li, unpublished observation). A similar pruning defect is found in *eff* mutants (26), raising the possibility that *eff*, the gene encoding the E2 ubiquitin-conjugating enzyme UbcD1, may function in the same genetic pathway. To test whether such a genetic interaction occurs in dendritic morphogenesis during larval development, we examined the dendritic branching phenotype in *dUBE3A* and *eff* transheterozygous larvae. Simultaneous loss of one copy of *dUBE3A* and one copy of *eff* had a more severe effect in reducing the number of terminal dendritic branches of ddaC neurons than that in *dUBE3A* or *eff* heterozygous larvae alone (Fig. 7). For this experiment, we used two different *eff* alleles ($eff^{mer4}$ and $eff^{s1782}$) and obtained similar results. Thus, UbcD1 and the dUBE3A may act in concert to regulate the levels of their target proteins, which in turn may influence dendritic growth and branching.

**The proper level of dUBE3A is critical for neuronal development**

To further understand the function of dUBE3A, we also cloned full length of dUBE3A and generated different UAS-*dUBE3A* transgenic fly lines. We overexpressed dUBE3A in different tissues using the UAS-Gal4 system and examined the developmental defects. Expression of dUBE3A in the *Drosophila* embryos by the tubulin-Gal4 led to a lethal phenotype at embryonic and early larval stages. Expression of dUBE3A in the developing nervous system by the *Elav*-Gal4, which is on the X chromosome, caused male lethality. We also expressed dUBE3A in the wing discs using the *vg*-Gal4 and observed a dramatic loss of wing margins (Fig. 7B). Expression of dUBE3A in the eye by the *GMR*-Gal4 caused a rough eye phenotype and a significant disorganization of omatidia in 1-day old flies (Fig. 7D) and degeneration of photoreceptors worsens over time (Fig. 7E). These findings suggest that increased expression of

dUBE3A can cause severe developmental defects. During the review process of our manuscript, Wu and colleagues (27) reported the generation of *dUBE3A* mutant flies and the overexpression phenotypes in the wing and the eye that are very similar to our findings presented here.

To examine the effects of dUBE3A expression on neuronal development, we targeted UAS-*dUBE3A* to a subset of DA sensory neurons using the $Gal4^{221}$. Interestingly, expression of dUBE3A decreased dendritic branching of ddaE and ddaF neurons (Fig. 9B), a phenotype similar to that caused by loss of dUBE3A activity. This finding suggests that the proper level of dUBE3A is critically important for the normal differentiation of neurons. We also expressed human UBE3A (hUBE3A) (20) in a subset of fly sensory neurons and observed a similar phenotype (Fig. 9C), suggesting a functional conservation in dendritic patterning.

## DISCUSSION

Since the mental retardation disorder AS is primarily caused by loss of the UBE3A protein product, it is of great importance to understand the normal function of UBE3A in neuronal development and synaptic plasticity. In this study, we used the P-element local hop-out approach to generate *dUBE3A*-null mutant fly lines. Although *UBE3A* knockout mice often die shortly after birth (15), *dUBE3A* mutant flies were viable to adulthood. The EP3214 line we obtained from the Bloomington Stock Center was homozygous lethal, but the lethality was probably not due to the EP insertion in the *dUBE3A* locus itself, as we could segregate the EP insertion from the background lethal mutation(s) after outcrosses with wildtype flies.

To understand the role of dUBE3A in neuronal development, we focused on the dendritic morphogenesis of DA neurons in the *Drosophila* PNS. One of the advantages of using DA neurons for phenotypic analysis is the ease of visualizing their dendrites in living animals. The dendritic trees of DA neurons are sandwiched between the epidermis and the body muscle wall

(28) and are essentially two-dimensional. Thus, the number of dendritic branches, especially their terminal fine processes, can be easily quantified at high resolution. Using this system, we found that loss of dUBE3A reduced the formation of terminal dendritic branches. This finding is consistent with the notion that dendritic pathology contributes to the pathogenesis of AS, as shown by the reduced length and density of dendritic spines in cerebellar, cortical, and hippocampal neurons and by the relatively normal appearance of dendritic trees stained with calbindin and examined by light microscopy (17). In *dUBE3A* mutant larvae, the major dendritic branches of ddaC neurons also appeared to be normal. Our finding that the development of terminal fine dendritic processes was affected by dUBE3A in *Drosophila* raises the possibility that this defect contributes to the neurological deficits in AS patients and mouse models. It is interestingly to note that overexpression of dUBE3A also decreased dendritic branching, which may have some implications for some forms of autism in which the genomic region containing *UBE3A* is duplicated (29). During the review process of this manuscript, Wu and colleagues reported independently the generation of *dUBE3A* mutant flies and their behavior phenotypes (27). It is plausible that dendritic developmental defects of CNS neurons in *dUBE3A* mutants may underlie, at least in part, the behavioral abnormalities of these flies.

Another advantage of the *Drosophila* model system is the ability to examine the cell-autonomous functions of a gene of interest (23). Our genetic analyses provide strong evidence that dUBE3A influences dendritic morphogenesis in a cell-autonomous manner. Dendritic pathology has been implicated in fragile X syndrome, Rett syndrome, and autism (30–34). Although the genes mutated in these neurodevelopmental disorders are different, including FMR1, an RNA-binding protein, MeCP2, a transcription regulator, and UBE3A, an E3 ubiquitin ligase, their downstream targets may participate in the same genetic pathways that regulate the formation of dendritic branches and dendritic spines. Loss of MECP2 activity leads to a

significant reduction in *UBE3A* expression in human brains (35). This finding may help explain the decreased dendritic branching and synaptogenesis caused by *MECP2* deficiency (36–39), However, *MECP2* knockout mice show normal levels of UBE3A (40), therefore, it seems that there is no direct genetic link between *MECP2* and *UBE3A*.

The substrates that are regulated by UBE3A and mediate its effects on dendritic development are still largely unknown. The Rho-GEF Pebble was identified as a candidate target for UBE3A in both flies and mice (20). However, expression of Pebble in *Drosophila* sensory neurons seemed to increase dendritic branching complexity (Y. Li, unpublished observation). Therefore, it is unlikely that the potential increase in Pebble expression could account for the decreased dendritic branching in *dUBE3A* mutant flies even though Pebble may well contribute to other cellular processes affected by dUBE3A. It is conceivable that dUBE3A may have many substrates, and elevated expression of some of them increases dendritic branching while others decrease dendritic branching. The availability of *dUBE3A*-null mutant flies and powerful genetic tools in this model system will facilitate the identification of UBE3A substrates that mediate its effect on a specific developmental process and may provide further insights into the molecular pathogenesis of AS.

## MATERIALS AND METHODS

### Fly Strains and Genetics

All flies were raised on standard food medium and kept at 25˚C. Line *EP3214* was from the Bloomington Stock Center and was homozygous lethal. To separate the background lethal mutation(s) from the EP insertion, we outcrossed *EP3214* with $w^{1118}$ for several generations and obtained adult viable lines homozygous for the EP insertion. The standard procedure for P-element hop-out was followed to generate genomic deletions in the *dUBE3A* locus.

$Gal4^{221}$ was used to label ddaE and ddaF neurons with GFP and drive the expression of UAS-*dUBE3A* RNAi constructs. To visualize ddaC neurons in third instar larvae, $Gal4^{477}$, UAS-*mCD8-GFP*/$Gal4^{477}$, UAS-*mCD8-GFP*; *TM3, Ser*/*TM6, Tb* flies were crossed with $dUBE3A^{\Delta 15-8}$/*TM3* or $dUBE3A^{\Delta 3-8}$/*TM3* flies to generate $Gal4^{477}$, UAS-*mCD8-GFP*/+; $dUBE3A^{\Delta 15-8}$/ $dUBE3A^{\Delta 15-8}$ or $Gal4^{477}$, UAS-*mCD8-GFP*/+; $dUBE3A^{\Delta 15-8}$/ $dUBE3A^{\Delta 3-8}$ third instar larvae for phenotypic analysis. For RNAi expression, $Gal4^{477}$, UAS-*mCD8-GFP*/$Gal4^{477}$, UAS-*mCD8-GFP*; *TM3, Ser*/*TM6, Tb* flies were crossed with UAS-RNAi lines from the VDRC to obtain $Gal4^{477}$, UAS-*mCD8-GFP*/+; *UAS-RNAi*/*TM6, Tb* flies, which were crossed with $dUBE3A^{\Delta 15-8}$/$dUBE3A^{\Delta 15-8}$ flies to select $Gal4^{477}$, UAS-*mCD8-GFP*/+; *UAS-RNAi, +/+,* $dUBE3A^{\Delta 15-8}$ third instar larvae for phenotypic analysis. Similar genetic crosses were performed to obtain *dUBE3A*, *eff* double heterozygous third instar larvae. The $eff^{mer4}$ allele was obtained from the Bloomington Stock Center. UAS-*hUBE3A* line was a gift of E. Bier (20). For expression in the eye, we used the *GMR*-Gal4. For expression in the wing, we used the *vg*-Gal4. Both lines were obtained from the Bloomington Stock Center.

MARCM analysis of DA neurons in the *Drosophila* PNS was performed as described (22). Briefly, the $dUBE3A^{\Delta 15-8}$ or $dUBE3A^{\Delta 3-8}$ mutations were recombined onto the chromosome

containing *FRT*$^{2A}$. *dUBE3A*$^{\Delta 15\text{-}8}$, *FRT*$^{2A}$*/TM3* or *dUBE3A*$^{\Delta 3\text{-}8}$, *FRT*$^{2A}$*/TM3* male flies were crossed with *Gal4*$^{C155}$, *UAS-mCD8-GFP*, *hs-FLP1*/*FM7* virgin flies. Then, *Gal4*$^{C155}$, *UAS-mCD8-GFP*, *hs-FLP1*; , *dUBE3A*$^{\Delta 15\text{-}8}$, *FRT*$^{2A}$/+ male flies were crossed with *Gal4*$^{C155}$, *UAS-mCD8-GFP*, *hs-FLP1*; *tubP-Gal80, FRT*$^{2A}$*/TM6,Tb* virgin flies. Embryos were collected on grape agar plates for 3 h at 25˚C, aged for 3 h, and heat-shocked in a 37˚C water bath for 40 min to induce mitotic recombination. The embryos were allowed to develop for 3–4 days in a moisture chamber at 25˚C. Third instar larvae containing a single mCD8-GFP-labeled dorsal cluster PNS neuron were selected under a Nikon fluorescence dissection microscope. A Nikon confocal microscope (D-Eclipse C1) was used to collect fluorescence images of dendritic morphology of single DA neurons. Dendritic termini were quantified as described (22). The data were analyzed by *t* test.

**Generation of dUBE3A antibody and RNAi lines**

Rabbit anti-dUBE3A antibody was generated against the first N-terminal 300 amino acids. For protein expression, DNA fragment of *dUBE3A* was amplified by PCR using specific primers (sense primer: 5’-ggaattcatgaacggtggcgggggtggc-3’; antisense primer: 5’-ccgctcgagttaatcatcgtc ctcttcttc-3’) and subcloned into *Eco*RI and *Xho*I sites of the pGEX4T1 vector. The GST-dUBE3A protein was purified with the GST-Fusion Protein Purification Kit (Pierce Biotechnology, Rockford, IL) and injected into rabbits for antiserum production (Covance, Princeton, NJ). Anti-dUBE3A antibody was purified from antiserum with the IgG Purification Kit (Pierce Biotechnology).

To generate two different UAS-*dUBE3A* RNAi constructs, each DNA fragment was amplified by PCR using specific primers (construct 1: sense primer 5’-atctcgagcaaatcctgtcgtaact gtc-3’ and antisense primer: 5’-catctagagcagcctaatcaagcgatac-3’; construct 2: sense primer 5’-tactcgagctgatcctcggcgaatttg-3’ and antisense primer 5’-gctctagagtcaaatacgagctataa cgg-3’) and

inserted into the *Xho*I and *Xba*I sites of the pUAST vector. To generate UAS-*dUBE3A* constructs, full-length dUBE3A coding region was amplified by PCR. These constructs were used to make transgenic flies.

***qRT-PCR Analysis***

Total RNA was extracted from homozygous adult male flies and purified with the RNeasy mini kit (Qiagen, Valencia, CA). The purified RNA was used as template to generate cDNA with Taqman reverse transcription reagent (Applied Biosystems, Foster City, CA). cDNA was used as template for qRT-PCR in a final volume of 25 µl. A standard curve was run in each PCR reaction. Individual values were normalized with the value of the gene encoding the ribosomal protein RP-49. Owing to the close proximity of the neighboring gene, *CG7600*, primers were also designed to detect *CG7600* transcripts. All reactions were performed three times in triplicate. Relative mRNA expression was calculated by using the standard curve method and the Delta-Delta Ct method.

***Western blot analysis***

Adult flies were frozen in a dry ice/ethanol bath and vortexed to remove heads. Heads were homogenized in RIPA buffer (0.137 M NaCl, 20 mM Tris HCl, pH 8.0, 10% glycerol, 1% NP-40, 0.1% SDS, 0.1% sodium deoxycholate) with 1 mM dithiothreitol and HALT Protease Inhibitor Cocktail (Pierce Biotechnology) and centrifuged to isolate total proteins. Protein concentrations were determined with the Bradford reagent (Bio-Rad, Hercules, CA).

For western blot analysis, ~40 µg protein was combined with 2X SDS loading buffer, resolved on an 8% SDS-PAGE gel, and transferred to polyvinylidine fluoride membranes. After blocking of nonspecific reactions in 5% nonfat milk in 0.1% TBST (25 mM Tris-HCl, 137 mM

NaCl, 3 mM KCl, pH 7.4, and 0.1% Tween-20), membranes were incubated in anti-dUBE3A (1:1000) for 2 h at room temperature. After washing with TBST, membrane blots were incubated in anti-rabbit-HRP secondary antibody (Jackson ImmunoResearch, San Jose, CA; 1:20,000) for 1 h at room temperature and detected with Supersignal West Pico (Pierce Biotechnology).

**ACKNOWLEDGEMENTS**

We thank J. Fischer, E. Bier, the Bloomington Stock Center, and the Vienna *Drosophila* RNAi Center for fly lines, T. Ahmad for helping with the fly eye sectioning, S. Ordway for editorial assistance and lab members for discussions and comments during the course of this work.

*Conflict of interest statement:* There are no conflicts of interest.

**FUNDING**

This study was supported by the Angelman Syndrome Foundation and the National Institutes of Health (F.-B.G.) (MH079198 and HD044752).

**REFERENCES**

1. Komiyama, T., Luo, L. (2006) Development of wiring specificity in the olfactory system. *Curr. Opin. Neurobiol*., **16**, 67–73.

2. Tada, T., and Sheng, M. (2006) Molecular mechanisms of dendritic spine morphogenesis. *Curr. Opin. Neurobiol*. **16**, 95–101.

3. Parrish, J.Z., Emoto, K., Kim, M.D., and Jan, Y.N. (2007) Mechanisms that regulate establishment, maintenance, and remodeling of dendritic fields. *Annu. Rev. Neurosci.,* **30**, 399–423.

4. Gao, F-B. (2007) Molecular and cellular mechanisms of dendritic morphogenesis. *Curr. Opin. Neurobiol*., **17**, 525–532.

5. Robb, S.A., Pohl, K.R.E., Wilson, B.J., and Brett, E.M. (1989) The "happy puppet" syndrome of Angelman: review of the clinical features. *Arch. Dis. Child.,* **64**, 83–86.

6. Jiang, Y.H., and Beaudet, A.L. (2004) Human disorders of ubiquitination and proteasomal degradation. *Curr. Opin. Pediatr*., **76**, 419–426.

7. Lalande, M., and Calciano, M.A. (2007) Molecular epigenetics of Angelman syndrome. *Cell. Mol. Life Sci*., **64**, 947–960.

8. Kishino, T., Lalande, M., and Wagstaff, J. (1997). UBE3A/E6-AP mutations cause Angelman syndrome. *Nat. Genet*., **15**, 70–73.

9. Matsuura, T., Sutcliffe, J.S., Fang, P., Galjaard, R.J., Jiang, Y.H., Benton, C.S., Rommens, J.M., and Beaudet, A.L. (1997) De novo truncating mutations in E6-AP ubiquitin-protein ligase gene (UBE3A) in Angelman syndrome. *Nat. Genet*., **75**, 74–77.

10. Huibregtse, J.M., Scheffner, M., and Howley, P.M. (1991) A cellular protein mediates association of p53 with the E6 oncoprotein of human papillomavirus types 16 or 18. *EMBO. J.,* **10**, 4129–4135.

11. Huibregtse, J.M., Scheffner, M., and Howley, P.M. (1993) Cloning and expression of the cDNAfor E6-AP, a protein that mediates the interaction of the human papillomavirus E6 oncoprotein with p53. *Mol. Cell Biol*., **73**, 775–784.

12. Albrecht, U., Sutcliffe, J.S., Cattanach, B.M., Beechey, C.V., Armstrong, D., Eichele, G., and Beaudet, A.L. (1997) Imprinted expression of the murine Angelman syndrome gene, UbeSa, in hippocampal and Purkinje neurons. *Nat. Genet.,* **77**, 75–78.

13. Rougeulle, C., Glatt, H., and Lalande, M. (1997) The Angelman syndrome candidate gene, UBE3A/E6-AP, is imprinted in brain. *Nat. Genet*., **77**, 14–15.

14. Vu, T.H., and Hoffman, A.R. (1997) Imprinting of the Angelman syndrome gene, UBE3A, is restricted to brain. *Nat. Genet*., **77**, 12–13.

15. Jiang, Y.H., Armstrong, D., Albrecht, U., Atkins, C.M., Noebels, J.L., Eichele, G., Sweatt, J.D., and Beaudet, A.L. (1998) Mutation of the Angelman ubiquitin ligase in mice causes

increased cytoplasmic p53 and deficits of contextual learning and long-term potentiation. *Neuron*, **27**, 799–811.

16. van Woerden, G.M., Harris, K.D., Hojjati, M.R., Gustin, R.M., Qiu, S., de Avila Freire, R., Jiang, Y.H., Elgersma, Y., and Weeber, E.J. (2007) Rescue of neurological deficits in a mouse model for Angelman syndrome by reduction of alphaCaMKII inhibitory phosphorylation. *Nat Neurosci.,* **10**, 280–282.

17. Dindot, S.V., Antalffy, B.A., Bhattacharjee, M.B., and Beaudet, A.L. (2008) The Angelman syndrome ubiquitin ligase localizes to the synapse and nucleus, and maternal deficiency results in abnormal dendritic spine morphology. *Hum. Mol. Genet.*, **17**, 111–118.

18. Bilen, J., and Bonini, N.M. (2005) *Drosophila* as a model for human neuro-degenerative disease. *Annu. Rev. Genet*., **39**, 153–171.

19. Bier, E. (2005) *Drosophila*, the golden bug, emerges as a tool for human genetics. *Nat. Rev. Genet.,* **6**, 9–23.

20. Reiter, L,T., Seagroves, T.N., Bowers, M., and Bier, E. (2006) Expression of the Rho-GEF Pbl/ECT2 is regulated by the UBE3A E3 ubiquitin ligase. *Hum. Mol. Genet*., **15**, 2825–2835.

21. Brand, A.H., and Perrimon, N. (1993) Targeted gene expression as a means of altering cell fates and generating dominant phenotypes. *Development*, **118**, 401–415.

22. Li W, Wang F, Menut L, Gao F-B. (2004). BTB/POZ-zinc finger protein Abrupt regulates dendritic branching in a neuronal subtype-specific and dosage-dependent manner. *Neuron,* **43**, 823–834.

23. Lee, T., and Luo, L. (1999) Mosaic analysis with a repressible cell marker for studies of gene function in neuronal morphogenesis. *Neuron,* **22**, 451–461.

24. Sweeney, N.T., Li, W. and Gao, F.B. (2002) Genetic manipulation of single neurons in vivo reveals specific roles of Flamingo in neuronal morphogenesis. *Dev. Biol*., **247**, 76–88.

25. Grueber, W.B., Jan, L.Y., and Jan, Y.N. (2002) Tiling of the *Drosophila* epidermis by multidendritic sensory neurons. *Development*, **129**, 2867–2878.

26. Kuo, C.T., Zhu, S., Younger, S., Jan, L.Y., and Jan, Y.N. (2006) Identification of E2/E3 ubiquitinating enzymes and caspase activity regulating *Drosophila* sensory neuron dendrite pruning. *Neuron*, **51**, 283–290.

27. Wu, Y, Bolduc, F.V., Bell, K., Tully, T., Fang, Y., Sehgal, A., and Fischer, J. A. (2008) A *Drosophila* model for Angelman syndrome. *Proc. Natl. Acad. Sci. USA*. **105**, 12399–12404.

28. Bodmer, R., Carretto, R., and Jan, Y. N. (1989) Neurogenesis of the peripheral nervous system in *Drosophila* embryos: DNA replication patterns and cell lineages. *Neuron,* **3**, 21–32.

29. Koochek, M., Harvard, C., Hildebrand, M. J., Van Allen, M., Wingert, H., Mickelson, E., Holden, J. J., Rajcan-Separovic, E., and Lewis, M. E. (2006) 15q duplication associated with autism in a multiplex family with a familial cryptic translocation t(14;15)(q11.2;q13.3) detected using array-CGH. *Clin. Genet*. **69**, 124–134.

30. Comery, T.A., Harris, J.B., Willems, P.J., Oostra, B.A., Irwin, S.A., Weiler, I.J., and Greenough, W.T. (1997) Abnormal dendritic spines in fragile X knockout mice: maturation and pruning deficits. *Proc. Natl. Acad. Sci. USA*, **94**, 5401–5404.

31. Belichenko, P.V., Oldfors, A., Hagberg, B., and Dahlström, A. (1994) Rett syndrome: 3-D confocal microscopy of cortical pyramidal dendrites and afferents. *Neuroreport*, **5**, 1509–1513.

32. Raymond, G.V., Bauman, M.L., and Kemper, T.L. (1996) Hippocampus in autism: a Golgi analysis. *Acta. Neuropathol.,* **91**, 117–119.

33. Kaufmann, W.E., and Moser, H.W. (2000) Dendritic anomalies in disorders associated with mental retardation. *Cereb. Cortex*., **10**, 981–991.

34. Zoghbi, H.Y. (2003) Postnatal neurodevelopmental disorders: meeting at the synapse? *Science*, **302**, 826–830.

35. Samaco, R.C., Hogart, A., and LaSalle, J.M. (2005) Epigenetic overlap in autism-spectrum neurodevelopmental disorders: MECP2 deficiency causes reduced expression of UBE3A and GABRB3. *Hum. Mol. Genet*., **14**, 483–492.

36. Matarazzo, V., Cohen, D., Palmer, A.M., Simpson, P.J., Khokhar, B., Pan, S.J., and Ronnett, G.V. (2004) The transcriptional repressor Mecp2 regulates terminal neuronal differentiation. *Mol. Cell. Neurosci*., **27**, 44–58.

37. Jugloff, D.G., Jung BP, Purushotham D, Logan R, Eubanks JH. (2005) Increased dendritic complexity and axonal length in cultured mouse cortical neurons overexpressing methyl-CpG-binding protein MeCP2. *Neurobiol. Dis*., **19**, 18–27.

38. Zhou, Z., Hong, E.J., Cohen, S., Zhao, W.N., Ho, H.Y., Schmidt, L., Chen, W.G., Lin, Y., Savner, E., Griffith, E.C., Hu, L., Steen, J.A., Weitz, C.J., and Greenberg, M.E. (2006) Brain-specific phosphorylation of MeCP2 regulates activity-dependent Bdnf transcription, dendritic growth, and spine maturation. *Neuron*, **52**, 255–269.

39. Smrt, R.D., Eaves-Egenes, J., Barkho, B.Z., Santistevan, N.J., Zhao, C., Aimone, J.B., Gage, F.H., and Zhao, X. (2007) Mecp2 deficiency leads to delayed maturation and altered gene expression in hippocampal neurons. *Neurobiol. Dis*., **27**, 77–89.

40. Jordan, C., and Francke, U. (2006) Ube3a expression is not altered in Mecp2 mutant mice. *Hum. Mol. Genet*., **15**, 2210–2215.

## FIGURE LEGENDS

**Figure 1.** Generation of *dUBE3A* mutant alleles. **(A)** Genomic organization of the *dUBE3A* locus. *dUBE3A* contains eight exons and is located on the chromosome 3L and flanked by genes *CG6199* and *CG7600*. Arrows indicate the direction of transcription. **(B)** Schematic of *dUBE3A* mutant alleles generated with the P-element local hop-out approach. An EP-element is inserted in the first exon of dUBE3A. Excision of this P-element resulted in the generation of deletion mutant alleles of *dUBE3A*. The size of each deletion was determined by sequencing of PCR fragments covering the deletion sites. In line *Δ15-8*, a 1156 bp fragment from the P-element remained in the first exon of *dUBE3A*, creating an insertional mutant allele.

**Figure 2.** Absence of *dUBE3A* expression in the mutant alleles. **(A)** Quantitative PCR (qPCR) analysis of relative mRNA levels of *dUBE3A* and *CG7600* in adult flies. Values are mean ± SEM. **(B)** Expression levels of dUBE3A protein in fly head extracts. Fly heads were used for western blot analysis because smaller dUBE3A fragments, presumably due to nonspecific degradation, were observed when protein extracts from whole flies were used (not shown). This polyclonal antibody recognized several nonspecific bands on western blot. However, the dUBE3A band of the predicted molecular weight was absent.

**Figure 3.** Dendritic phenotypes of ddaC neurons in *dUBE3A* mutant third instar larvae. GFP expression in ddaC neurons was under the control of $Gal4^{477}$. **(A)** $Gal4^{477}$, *UAS-mCD8-GFP/+; +/+* larvae were used as controls. **(B, C)** Dendritic phenotypes were analyzed in $Gal4^{477}$, *UAS-mCD8-GFP/+;* $dUBE3A^{\Delta 15\text{-}8}/dUBE3A^{\Delta 15\text{-}8}$ **(B)** and $Gal4^{477}$, *UAS-mCD8-GFP/+;* $dUBE3A^{\Delta 15\text{-}8}/dUBE3A^{\Delta 3\text{-}8}$ **(C)** larvae at the third instar stage. **(D)** Quantification of the number of dendritic termini of ddaC neurons for genotypes in **A–C**. Values are mean ± SEM. $***P < 0.001$.

**Figure 4.** Genetic analysis of dUBE3A function in dendritic morphogenesis using the RNAi approach. **(A)** Western blot analysis of dUBE3A expression in extracts of heads from adult control flies, *dUBE3A*$^{\Delta 15\text{-}8}$ homozygous mutants, and flies expressing different UAS-RNAi constructs under the control of *tubulin-Gal4*. UAS-RNAi lines *2-3, 8-2, 9-1, 29-1*, and *29-10* were generated in our laboratory; *45875* and *45876* were from the VDRC. The bracket indicates the non-specific bands recognized by the dUBE3A polyclonal antibody. ** indicates dUBE3A; the top band is likely a post-translationally modified form. **(B)** A wildtype ddaC neuron in the A3 segment of a third instar larva. The number of dendritic ends of ddaC neurons in *dUBE3A*$^{\Delta 15\text{-}8}$/+ is slightly reduced (See Fig. 7). **(C)** A ddaC neuron expressing UAS-*dUBE3A* RNAi (VDRC45875) in the *dUBE3A*$^{\Delta 15\text{-}8}$/+ background. **(D)** A ddaC neuron expressing UAS-*dUBE3A* RNAi (VDRC45876) in the *dUBE3A*$^{\Delta 15\text{-}8}$/+ background. **(E)** Quantification of dendritic ends from ddaC neurons in the A3 segment from larvae in panels **B–D**. Values are mean ± SEM. ***$P < 0.001$.

**Figure 5**. MARCM analysis of the cell-autonomous function of *dUBE3A* in the dendritic morphogenesis of ddaC neurons. **(A)** A control ddaC neuron in the A3 segment of a third instar larva. **(B)** A *dUBE3A*$^{\Delta 3\text{-}8}$ homozygous mutant ddaC neuron in the A3 segment of a third instar larva. **(C)** A *dUBE3A*$^{\Delta 15\text{-}8}$ mutant ddaC neuron. **(D)** Quantification of the number of terminal dendritic branches from ddaC neurons with the genotypes of **A–C**. Values are mean ± SEM. *$P < 0.05$; ***$P < 0.001$.

**Figure 6**. Cell-autonomous effects of *dUBE3A* on dendritic branching in ddaE and ddaF neurons. **(A)** A control ddaE neuron labeled by GFP. **(B)** A ddaE neuron homozygous for the

*dUBE3A*$^{\Delta 3\text{-}8}$ allele. **(C)** A ddaE neuron homozygous for the *dUBE3A*$^{\Delta 15\text{-}8}$ allele. The GFP-labeled ddaE neurons in **A–C** were generated by the MARCM technique. **(D)** Quantification of the number of dendritic branches of ddaE and ddaF neurons of different genotypes. **(E)** A wildtype ddaE and a wildtype ddaF neuron labeled by GFP under the control of *Gal4*$^{221}$. **(F)** A ddaE and a ddaF neuron expressing UAS-*dUBE3A* RNAi (VDRC45876) driven by *Gal4*$^{221}$. **(G)** A ddaE and a ddaF neuron expressing UAS-*dUBE3A* RNAi (VDRC45875) driven by *Gal4*$^{221}$. **(H)** Quantification of the number of dendritic branches of ddaE and ddaF neurons expressing GFP and RNAi constructs. Values are mean ± SEM. *$P < 0.05$; ***$P < 0.001$.

**Figure 7**. Genetic interaction between *dUBE3A* and *eff* in dendritic morphogenesis. **(A)** A control ddaC neuron in the A3 segment of a third instar larva. **(B)** A ddaC neuron in a heterozygous *dUBE3A*$^{\Delta 15\text{-}8}$/+ third instar larva. **(C)** A ddaC neuron in a heterozygous *eff*/+ third instar larva. **(D)** A ddaC neuron in a transheterozygous *dUBE3A*/*eff* third instar larva. **(E)** Quantification of the number of dendritic termini of ddaC neurons in different genetic backgrounds. Values are mean ± SEM. *$P < 0.05$, ***$P < 0.001$.

**Figure 8**. dUBE3A overexpression phenotypes in the wing and the eye. (**A**) A wildtype wing from a 3-day old *vg*-Gal4 fly. (**B**) A wing expressing dUBE3A under the control of the *vg*-Gal4. (**C**) A section of an eye from a 3-day old *GMR*-Gal4 fly showing the regular arrangement of omatidia. (**D**) A section of an eye from a 1-day old fly expressing dUBE3A under the control of *GMR*-Gal4. (**E**) A section of an eye from a 7-day old fly expressing dUBE3A by the *GMR*-Gal4 showing extensive retinal degeneration.

**Figure 9**. The effects of ectopic expression of dUBE3A and hUBE3A on dendritic branching of a subset of *Drosophila* sensory neurons. (**A**) Wildtype ddae and ddaF neurons are labeled by GFP under the control of the $Gal4^{221}$. (**B**) A representative image of ddaE and ddaF neurons that express dUBE3A. (**C**) A representative image of ddaE and ddaF neurons that express hUBE3A. (**D**) Quantifications of the number of dendirtic ends of ddaE and ddaF neurons with different genetic backgrounds as in A–C. Values are mean ± SEM. $*P < 0.05$; $**P < 0.01$; $***P < 0.001$. The sample numbers for each genotype are listed in the middle of each column.

Fig. 1

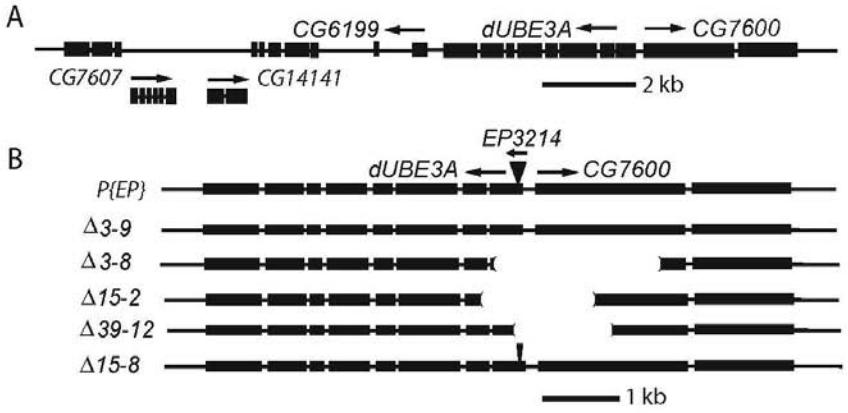
A
CG6199
dUBE3A
CG7600
CG7607
CG14141
2 kb
B
EP3214
dUBE3A
CG7600
P{EP}
Δ3-9
Δ3-8
Δ15-2
Δ39-12
Δ15-8
1 kb

Fig. 2

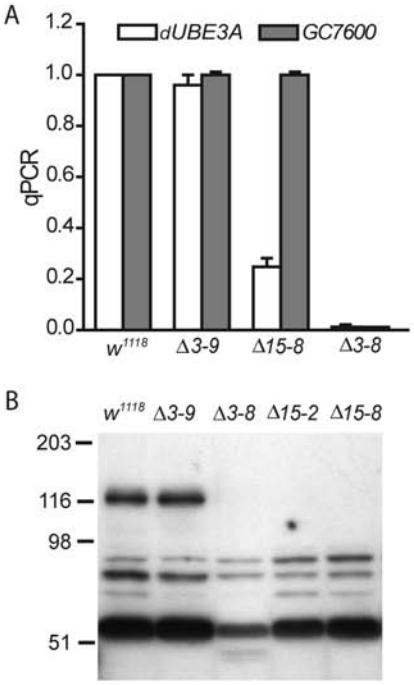
A
dUBE3A
GC7600
qPCR
1.2
1.0
0.8
0.6
0.4
0.2
0.0
w1118
Δ3-9
Δ15-8
Δ3-8
B
w1118
Δ3-9
Δ3-8
Δ15-2
Δ15-8
203
116
98
51

Fig. 3

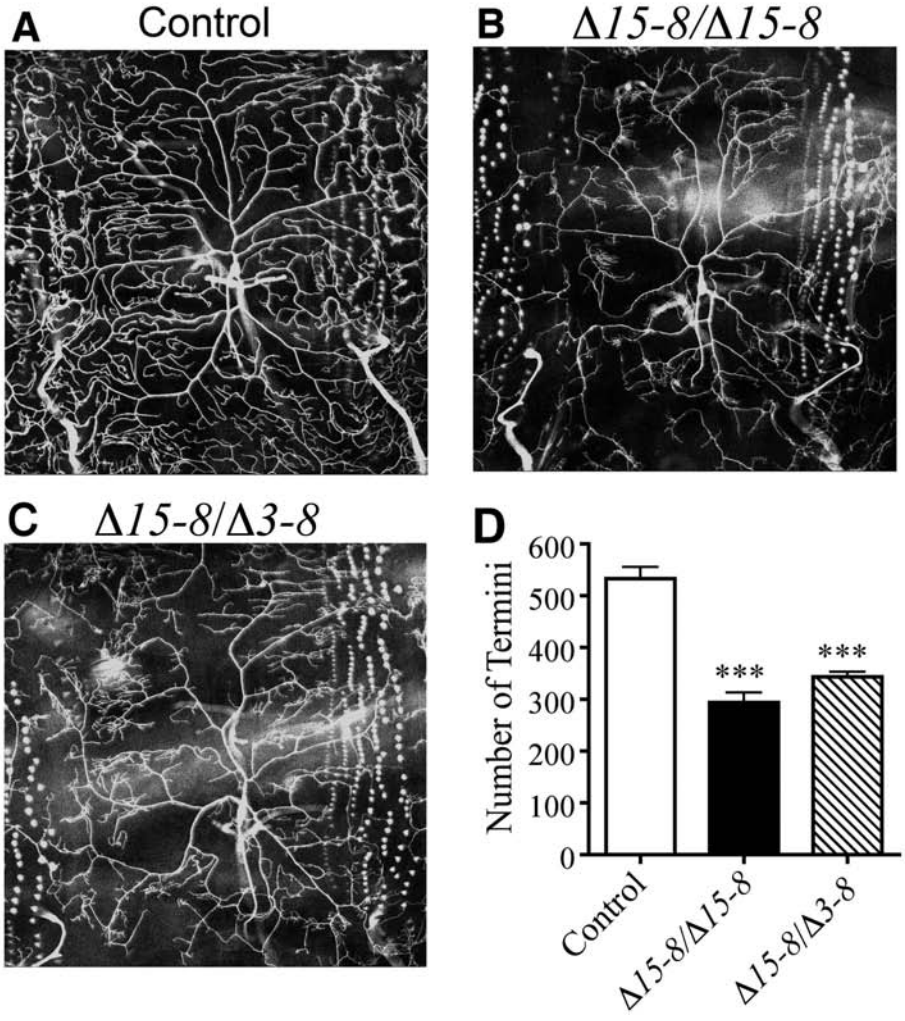
A
Control
B
Δ15-8/Δ15-8
C
Δ15-8/Δ3-8
D
Number of Termini
600
500
400
300
200
100
0
***
***
Control
Δ15-8/Δ15-8
Δ15-8/Δ3-8

Fig. 4

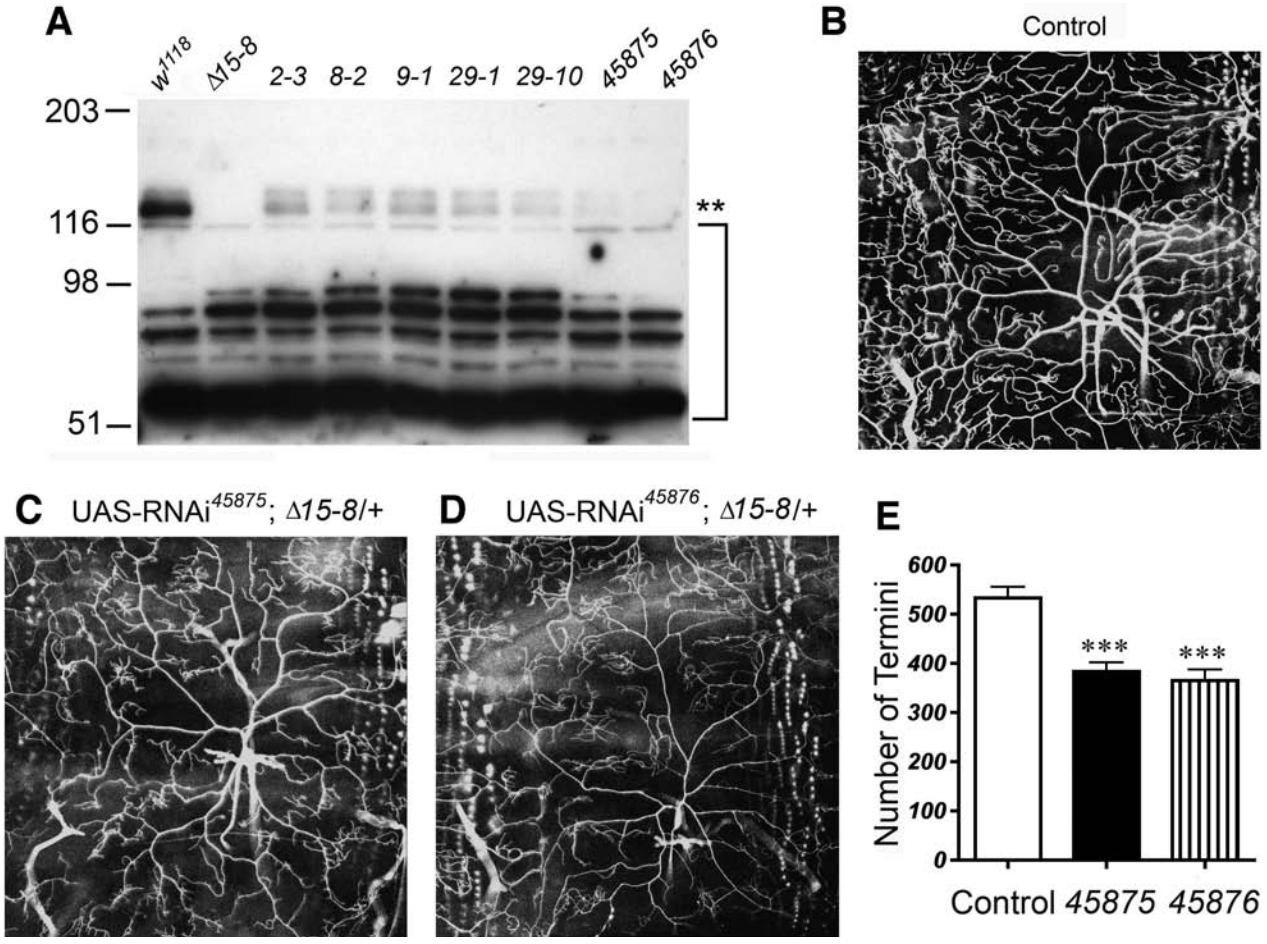
A
w1118
Δ15-8
2-3
8-2
9-1
29-1
29-10
45875
45876
203
116
98
51
**
B
Control
C
UAS-RNAi45875; Δ15-8/+
D
UAS-RNAi45876; Δ15-8/+
E
Number of Termini
600
500
400
300
200
100
0
***
***
Control
45875
45876

Fig. 5

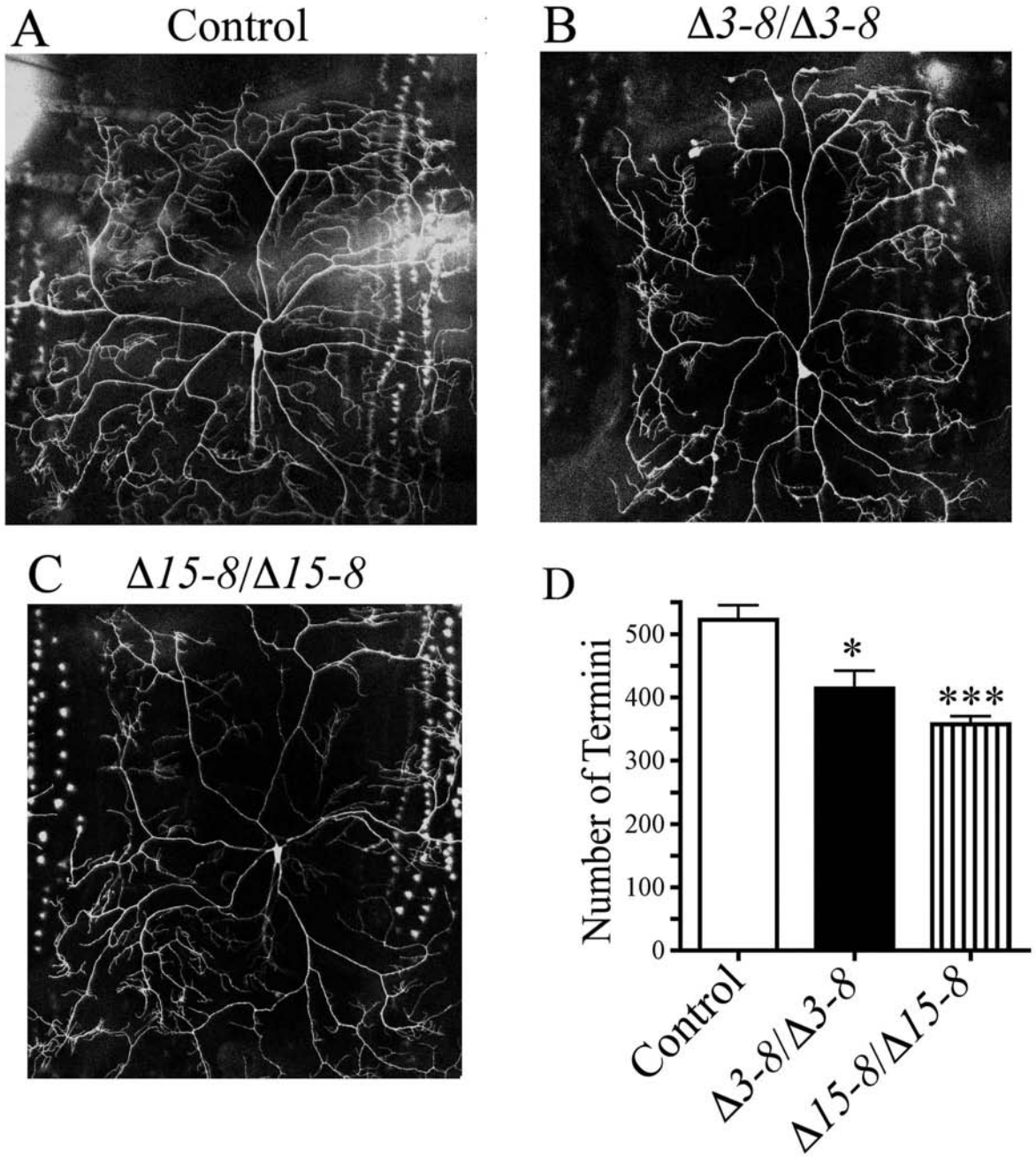
A
Control
B
Δ3-8/Δ3-8
C
Δ15-8/Δ15-8
D
Number of Termini
500
400
300
200
100
0
*
***
Control
Δ3-8/Δ3-8
Δ15-8/Δ15-8

Fig. 6

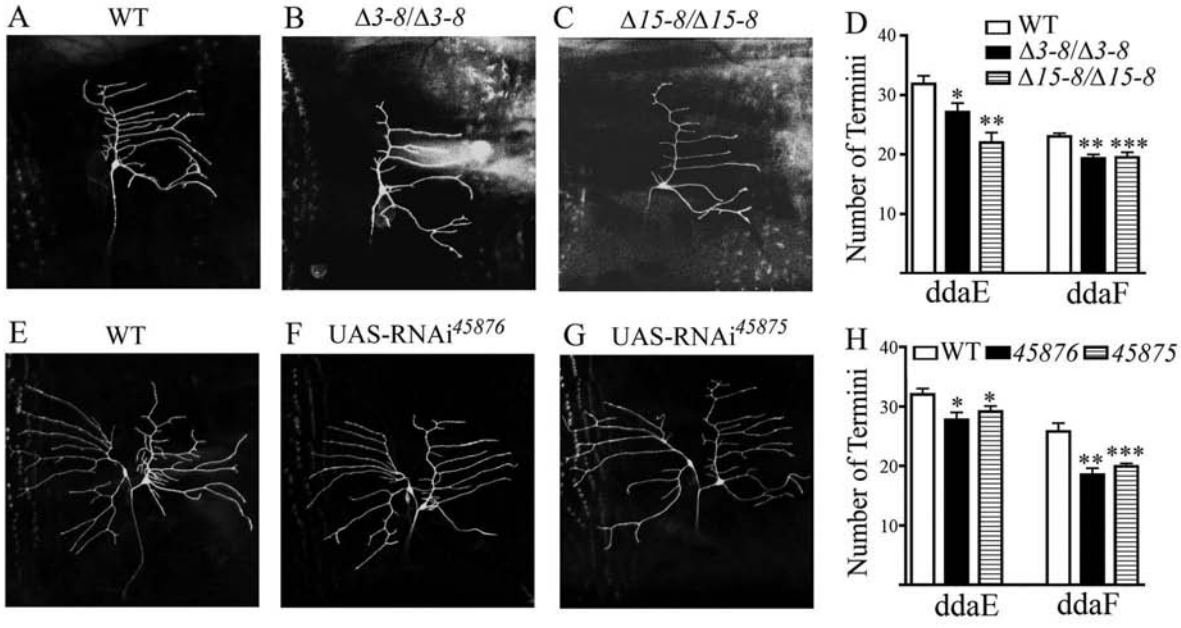
A WT
B Δ3-8/Δ3-8
C Δ15-8/Δ15-8
D
WT
Δ3-8/Δ3-8
Δ15-8/Δ15-8
Number of Termini
40
30
20
10
*
**
**
***
ddaE
ddaF
E WT
F UAS-RNAi45876
G UAS-RNAi45875
H
WT
45876
45875
Number of Termini
40
30
20
10
*
*
**
***
ddaE
ddaF

Fig. 7

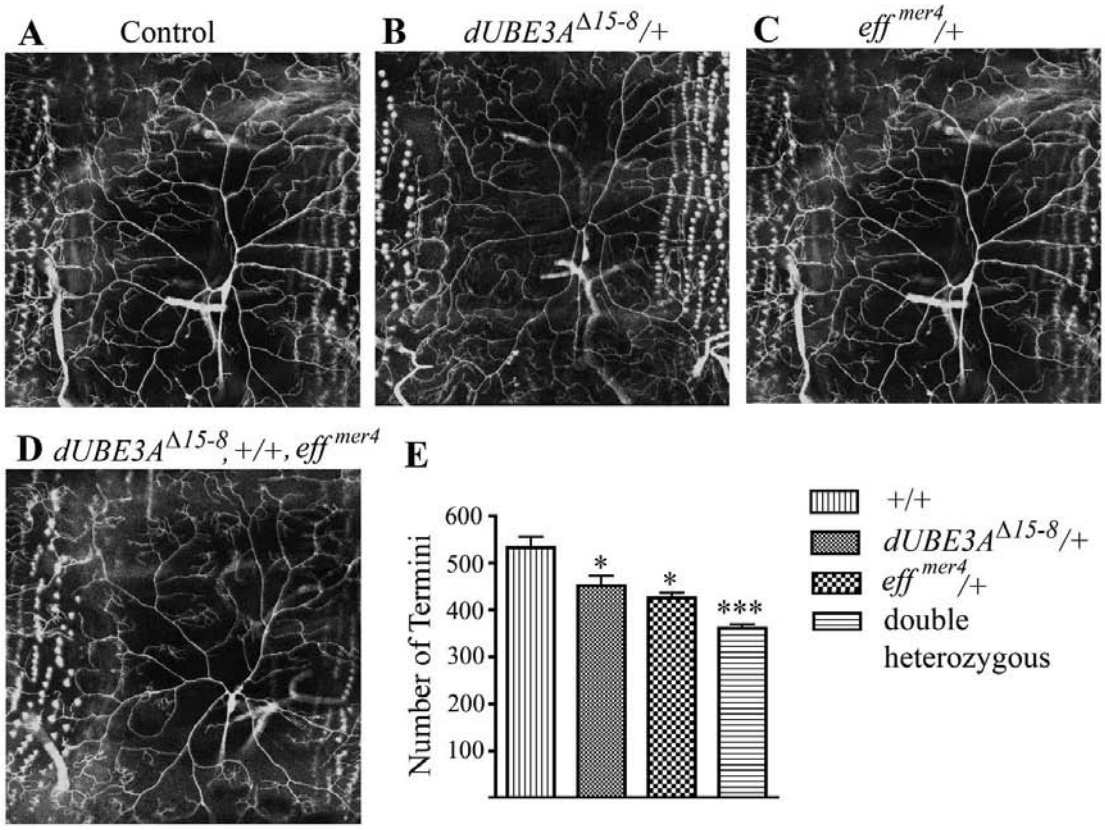
A Control
B dUBE3A^Δ15-8/+
C eff^mer4/+
D dUBE3A^Δ15-8;+/+, eff^mer4
E
Number of Termini
600
500
400
300
200
100
*
*
***
+/+
dUBE3A^Δ15-8/+
eff^mer4/+
double heterozygous

Fig. 8

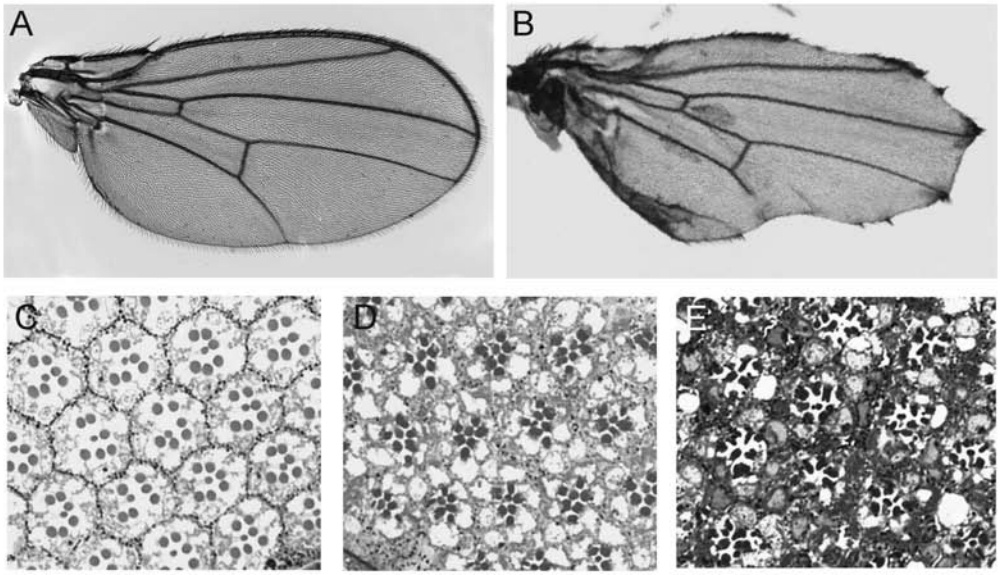

Fig. 9

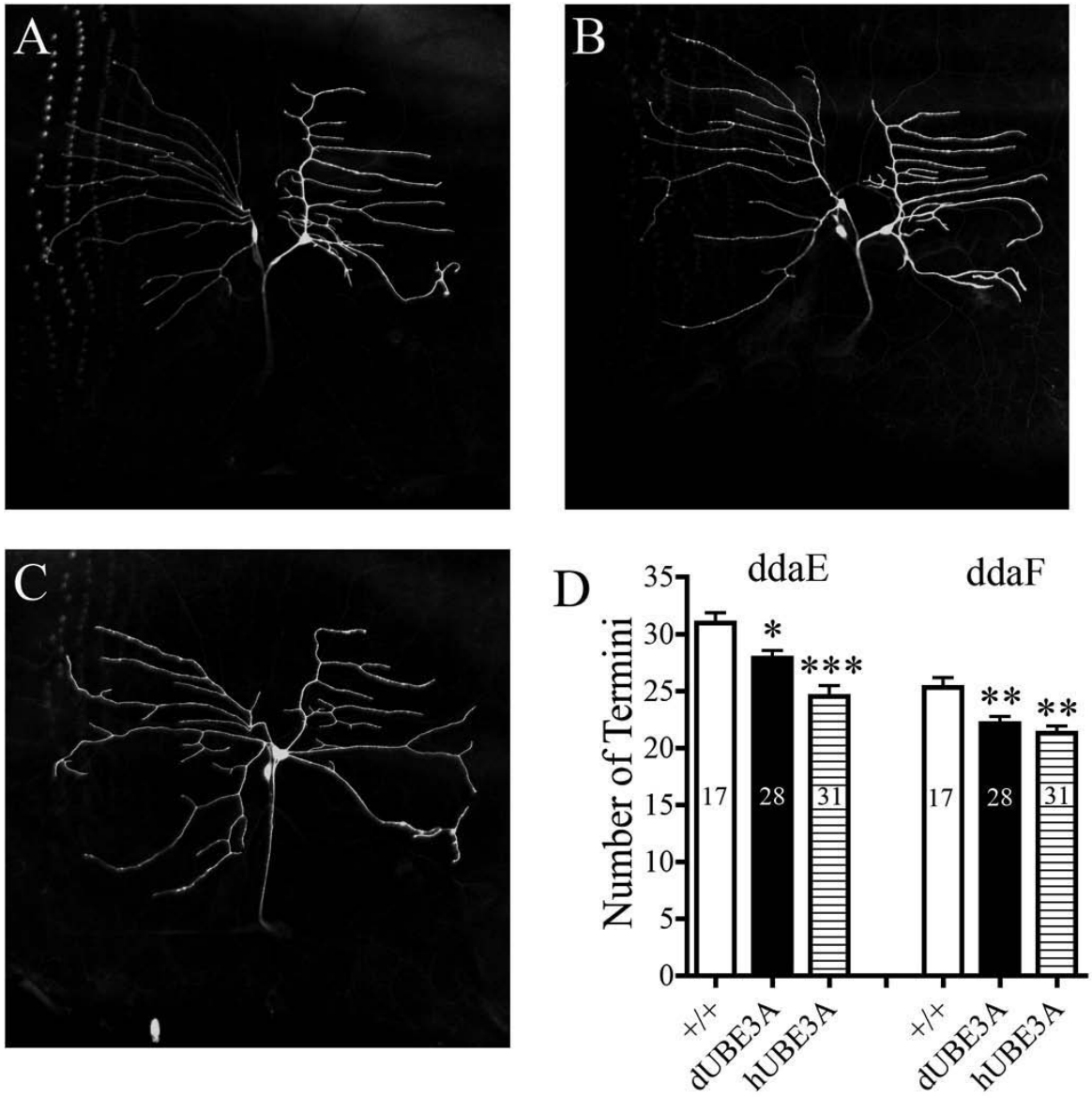
A
B
C
D
ddaE
ddaF
Number of Termini
35
30
25
20
15
10
5
0
*
***
**
**
17
28
31
17
28
31
+/+
dUBE3A
hUBE3A
+/+
dUBE3A
hUBE3A